An Energy Scheduling Algorithm Supporting Power Quality Management in Commercial Building Microgrids

M. Hong, X. Yu, N. Yu and K. A. Loparo

Abstract **- This paper presents an energy scheduling algorithm for a small-scale microgrid serving small to medium size commercial buildings (the Building Microgrid) that includes conventional and renewable distributed generation resources, energy storage, and both linear and nonlinear loads. An essential study objective is to mitigate power quality issues through coordinating the operating schedules of sensitive devices in the Building Microgrid. The proposed energy scheduling algorithm is formulated as a mixed integer programming problem where power quality requirements are modeled in the constraints. The algorithm also involves validation with the harmonics and dynamic event simulations. Case studies have been performed with realistic model parameters to verify the performance of the algorithm. The study results demonstrate the effectiveness of the algorithm in managing voltage and frequency deviations, as well as harmonic distortions. In the transaction-based control framework, the proposed algorithm can be used to aggregate device transaction bids and facilitate the buildings-to-grid integration.**

Index Terms **- Microgrid, distribution generation, transaction-based framework, buildings-to-grid integration, power quality, harmonic distortions.**

I. INTRODUCTION

IN recent years, microgrid technologies have captured global interests among governments, industries and academic institutions due to their potential benefits in improving energy efficiency and reliability, and reducing carbon emissions. Although a strict definition of microgrid does not exist, it is generally agreed that a microgrid system should be a single controllable entity that operates in both grid-connected and standalone modes of operation [1]. Meanwhile, the total generation capacity, operational capabilities and network boundary of a microgrid system can vary, depending on the end-use entity being served. Microgrid systems have been built on university campuses, military installations and other industrial sites, for supporting both demonstration and mission-critical activities.

This study effort investigates the energy scheduling problem of small-scale microgrid systems, such as those serving small to medium size commercial buildings. Such a microgrid system involves mainly the low voltage distribution system network, and can serve a peak load capacity of up to 1 MW. These microgrid systems are referred to as *Commercial Building Microgrids* in some recent literature [2~4], or *Building Microgrids* in this study.

One of the primary operational challenges in a Building Microgrid is associated with power quality management when the microgrid is in standalone operation. Due to the small generation capacity, the physical operating characteristics of building equipment and appliances can considerably affect the microgrid voltage, current and frequency, and result in harmful harmonic distortions. Therefore, the device operating characteristics must be adequately modeled in both the fast time scales associated with local controls and the longer time scales relevant to energy scheduling.

This paper proposes a Mixed Integer Programming (MIP) based energy scheduling algorithm where power quality requirements are formulated as constraints. Considerable discussions are also held around the hierarchical control schemes for ensuring the operational feasibility of the energy schedules. Both fast and longer time scale case studies have been performed with realistic model parameters to verify the energy scheduling outcome. The study results show that the proposed algorithm can effectively improve the microgrid operation to meet power quality requirements, especially in managing voltage and current harmonic distortions for sensitive devices. The unique contributions of this work are in identification of power quality related operational issues in Building Microgrids, and the proposed modeling and mitigation approaches through the microgrid long term energy scheduling.

This study is primarily motivated by recent development in building technologies such as intelligent Building Automation Systems (BAS) that can leverage distributed sensing and control technologies to achieve improved operational and economic objectives. Meanwhile, buildings-to-grid integration has been identified as an essential way of improving the efficiency of energy supply and demand, as buildings in the United States consumes nearly 40% of total energy [5]. The *Transaction-Based Framework* [6, 7] is a promising technology for buildings-to-grid integration where demands are aggregated at various tier levels of energy management, and interact with grid energy prices. This study identifies the Building Microgrid as a crucial enabling technology for implementing the transaction-based framework at the end-user tier level. This is accomplished by integrating the operations of BAS and on-site DG capacity to effectively facilitate energy transactions among end-use devices and the grid. In the transaction-based framework, the proposed energy scheduling algorithm can aggregate the transaction bids of building devices while meeting local operational and economic objectives.

This study is also motivated by the underutilization of backup generation capacities in building facilities as distributed generation (DG). Commercial buildings with critical loads are often equipped with on-site backup generation, such as diesel generator sets or batteries. Typically, backup generators are used to only serve designated critical loads. In many cases, backup generators are oversized in capacity to meet the power quality requirements for the served loads and only operate under emergency conditions [8]. This study shows that integrating

---

M. Hong and K. A. Loparo are with the Case Western Reserve University, Cleveland, OH 44106. (mingguo.hong@case.edu and kenneth.loparo@case.edu.)
X. Yu is with Xi'an University of Technology, Xi'an, China (yuxiangyang0@gmail.com). N. Yu is with the University of California Riverside, California (eric.ynp@gmail.com).
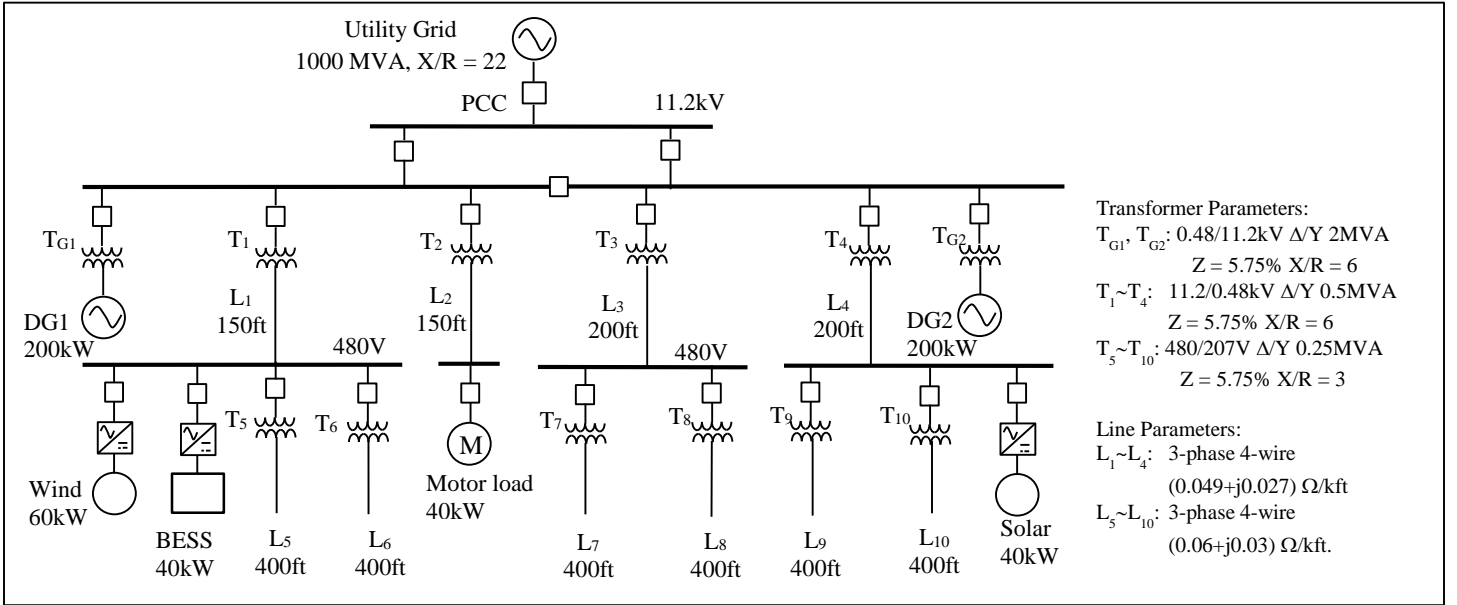
Figure 1: The Building Microgrid Model

backup generation in microgrid operation will significantly improve their utilization.

In the remaining presentation, section II describes a realistic Building Microgrid model; section III describes a hierarchical control framework for the microgrid power and energy management, and a Multi-Agent System (MAS) based implementation platform; section IV identifies the power quality issues in Building Microgrid operation; section discusses the MIP based energy scheduling algorithm; and the case studies are presented in section VI, followed by conclusions in section VII.

II. THE BUILDING MICROGRID MODEL

The Building Microgrid model for this study is based on a section of the Case Western Reserve University (CWRU) campus grid that includes three campus buildings served by the medium-voltage campus electric distribution system [9]. As shown in Figure 1, the 11.2 kV voltage network includes two busses connected by a short distance cable line. The rest of the network consists of step-down transformers (11.2kV/480V and 480/207V) and distribution cables that connect to various building breaker panels. The distribution system networks beyond the breaker panels are not represented in the model. Also, two 200 kW natural gas backup generator sets (DG1 and DG2) are connected to the Point of Common Coupling (PCC) bus of the microgrid. Three additional DG resources are added to the microgrid model, including a 60 kW wind generation unit, a 40 kW solar generation unit, and a 40 kW battery energy storage system (BESS) unit. The capacity specifications of these DG resources have been based on realistic considerations about the building premise, such as available rooftop area for placing solar panels and open air space to install the wind turbine. The BESS unit is sized to adequately supply critical loads in the buildings for about two consecutive hours when no other generation source is available. These critical loads include the hallway lighting and emergency alarm systems.

The main electric loads in the Building Microgrid are motors, lighting and plug loads. A BAS exists with sensors and controls both at the device level for large electric equipment such as an elevator, and at the aggregate level (at a breaker panel) for smaller appliances such as hallway lights. Therefore, a load defined in this study is an electric end-use entity monitored and controlled by the BAS, which represents either an individual device or an aggregate of devices. A total of 75 loads are considered, with capacities ranging from 5 to 40 kW. These loads can be in either three phases or single phase, distributed along the lines downstream from the distribution transformers. Among the total load capacities, there are:

- Linear loads that represent individual or aggregates of linear loads, such as incandescent lamps, space heaters, etc.
- Nonlinear loads that represent individual nonlinear, or mix of linear and nonlinear loads involving fluorescent lights, power electronic switching such as variable speed drives, switch mode power supplies (SMPS), and computers.
- Duty-cycle motor loads, such as refrigeration facilities and elevators (which are nonlinear as well).

Among the various nonlinear loads, the harmonic spectrums associated with nonlinear lighting, electronics, and other refrigeration equipment are defined based on the findings of [10]. The sensitive load requirements on voltage sag and harmonic distortions are defined based on typical industry practice [11].

III. POWER AND ENERGY MANAGEMENT IN BUILDING MICROGRIDS

A. A Hierarchical Control Strategy

In general, the control systems for the power and energy management of a microgrid can be organized in a three-tier hierarchical structure, based on the time scales of control responses. The primary controls include the local controls for frequency and voltage regulations that can respond on time scales of milliseconds; the secondary controls are steady state set points provided to the primary controls on periodicities from a few seconds up to a few minutes, usually by a centrally executed algorithm; and the tertiary controls concern the energy scheduling decisions over longer planning time horizons.
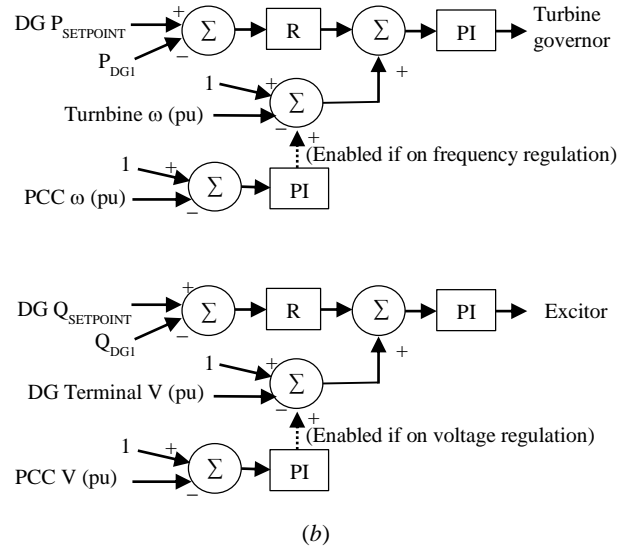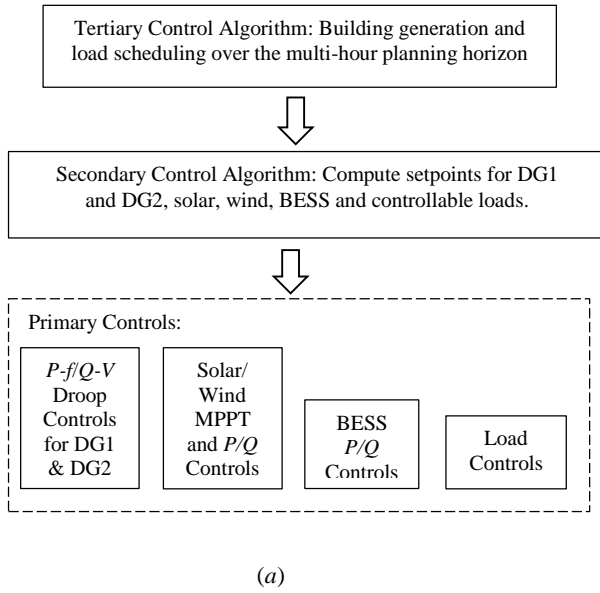
Figure 2: Hierarchical Controls of the Building Microgrids

Depending on the microgrid system capacity, network configuration and generation technology, various challenges can be encountered in applying hierarchical controls to microgrids, especially with the design of primary controls. For example, in microgrids where the DG resources are separated by a resistive network, the primary droop controls for frequency and voltage regulations become very difficult to implement due to the coupling between active and reactive powers [12]. High-bandwidth, site-to-site communication may be required to coordinate the primary controls to enable power sharing among the DG resources. In addition, in microgrids where the dominant generation resources are invertor based, there are significant complications in filtering harmonic contents to obtain valid control signals [12]. These challenges of microgrid control can be successfully addressed for a Building Microgrid, as DG resources are within close proximity to each other, with fossil-fuel based generation sets primarily to meet the capacity requirements. As a result, conventional droop control methods, such as active power-frequency (*P-f*) and reactive power-voltage (*Q-V*) can be successfully implemented on fossil-fuel DGs for voltage and frequency regulations. One of the most outstanding challenges with controls in the Building Microgrid, however, are associated with power quality management.

The proposed hierarchical control structure for the Building Microgrid is illustrated by the diagram of Figure 2 (*a*). Each of the three control layers are further discussed in the following.

B. Primary Controls

The primary controls of the building micrgrid consist of the local controls of the generation resources and BESS units that are capable of following setpoint instructions. They are:

a. Turbine governor *P-f* and exciter *Q-V* droop controls for the fossil fuel based synchronous generator sets (Figure 2 (*b*)). The generator sets can operate either in the frequency and voltage regulation mode, or in the active power and reactive power (*P/Q*) control mode.

b. Wind generation Maximum Power Point Tracking (MPPT) and *P/Q* controls.

c. Solar generation MPPT and *P/Q* controls.

d. BESS *P/Q* controls.

With local measurements taken on generator rotor frequency and terminal voltage, the *P-f/Q-V* droop controls enable active and reactive power sharing among DG1 and DG2. For the solar and wind generators, they can either operate in the MPPT mode, or follow *P* and *Q* setpoints in the *P/Q* control mode. The charge and discharge rates of the BESS unit should follow the *P* and *Q* setpoints.

C. Secondary and Tertiary Controls in a MAS Framework

The secondary control algorithm determines the setpoints for all primary controls, as well as the on/off statuses and power consumption levels for the controllable loads. The secondary control setpoints for the generation units and loads reflect the energy operation schedule as determined by the tertiary control algorithm of advance planning. Certain discrepancies will occur, however, between the planned and actual operation schedules due to wind and solar forecast errors or actual load consumption deviations from the planned schedule. In real time operation, the secondary control maintains active and reactive power balance through adjusting the power outputs of fossil fuel generation units DG1 and DG2. When the microgrid is in the grid-connected mode of operation, DG1 and DG2 are placed on *P/Q* control mode where the setpoints are provided by the secondary control as a result of economic dispatch; in the standalone mode, DG1, DG2 or both units should provide frequency and voltage regulations and the setpoints are again determined by the secondary control (which are typically 1 per unit of their nominal ratings, i.e., 60 HZ and 11.2 kV as measured at the PCC. See Figure 2 (*b*)).

The tertiary control algorithm supporting power quality management is the main focus of this presentation and will be separately discussed in sections IV, V and VI. The essential cyber infrastructure for implementing the secondary and tertiary controls is the MAS-based platform VOLTTRON, developed by
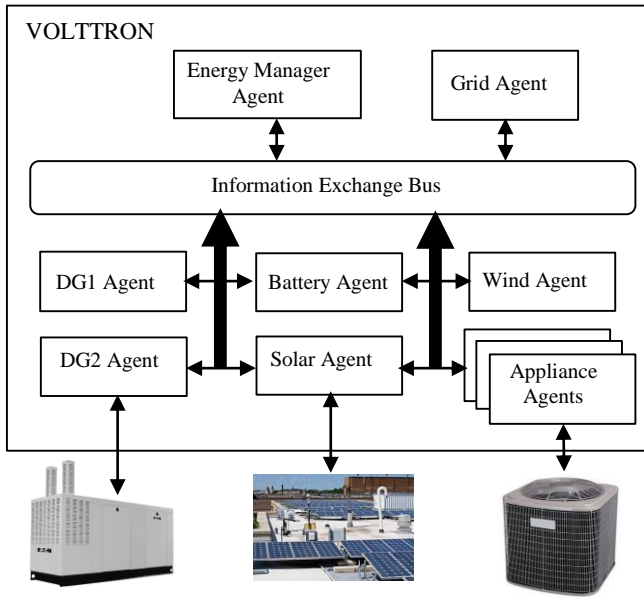
Figure 3: VOLTTRON as the multi-agent system platform

the Pacific Northwest National Laboratory (PNNL) to facilitate transactive controls for building automation and buildings-to-grid integration [13]. In this framework, agents are instantiated in VOLTTRON to represent the building energy manager, grid, and various devices such as generation resources and BESS unit, as well as building equipment and appliances (Figure 3). A device agent is able to retrieve sensor measurement data from the represented device and also issue control commands such as setpoints to the device through the BACNET protocol. Both the secondary and tertiary control algorithms are implemented in the Energy Manager agent that carries out two-way communication with other agents in order to make energy management decisions. For example, in real time operation, the Energy Manager agent collects sensor measurements from other agents and also determines the device setpoints to ensure power balance in the microgrid. During the energy planning of the tertiary control, additionally, the device agents submit electronic bids that represent both the prices and capacities for which they are willing to produce or consume energy. The Energy Manager agent then clears the bids through executing a central energy scheduling algorithm and informs the device agents on the resultant energy schedules. Currently, development effort is undergoing at CWRU to use VOLTTRON as the MAS platform for the energy management system of a Building Microgrid.

IV. POWER QUALITY ISSUES IN THE BUIDLING MICROGRID

Power quality issues remain to be outstanding in the standalone operation of small-scale microgrids, such as the Building Microgrid. Effective mitigation of the issues is among the key objectives of microgrid control.

A. Harmonic Distortions

The primary sources for the voltage and current harmonic contents are the nonlinear loads. When the microgrid is operating in the grid-connected mode, voltage and current harmonic distortions are limited due to the stiffness of the grid source and grid code compliance requirement [14]. When the microgrid is operating in the standalone mode, voltage and current harmonic distortions become significantly higher. High

harmonic contents not only limit the maximum loading levels of the DGs, but also affect the performance of sensitive loads.

As harmonic currents from nonlinear loads propagate through the microgrid system, they can become attenuated or canceled due to the network impedance and special configurations such as delta transformer windings [17]. Two important measures are defined to identify the extent of harmonic distortion: the Total Harmonic Distortion (THD) as the percentage of the root mean square (RMS) of the harmonic frequency components against the fundamental frequency component, and the Total Demand Distortion (TDD) as the percentage of the RMS of the harmonic frequency current against the rated load current. THD is the most effective measure for the impact of harmonic distortions in voltage, while TDD is the most effective measure for the impact of harmonic distortions in current.

$$V_{THD} = \frac{\sqrt{V_2^2 + V_3^2 + ... + V_h^2}}{V_1} \; , I_{TDD} = \frac{\sqrt{I_2^2 + I_3^2 + ... + I_h^2}}{I_{rated}} \quad (1), (2)$$

where V_h and I_h represent the RMS values of various order harmonic contents in voltage and current.

In order to study the propagation of harmonic currents in the network, the following sensitivity factors have been defined in this study. For certain load l, network branch br, node n, and operation hour h:

$$\omega(br,l,h) = \frac{\partial I_{TDD}(br,h)}{\partial P(l,h)} \; , \; \mu(n,l,h) = \frac{\partial V_{THD}(n,h)}{\partial P(l,h)} \quad (3), (4)$$

in kW^{-1}, where

- $I_{TDD}(br, h)$ represents the branch current TDD in percentage associated with branch br during hour h.
- $V_{THD}(n, h)$ represents the nodal voltage THD in percentage associated with node n during hour h.
- $P(l, h)$ represents the active power draw of load l of a given harmonic spectrum.

Sensitivity factors $\omega(br, l, h)$ and $\mu(br, l, h)$ are nonlinear functions of the distributed network loads, whose analytical expressions are to be further developed in future research. This study takes a numerical approach by estimating their values using the perturbation method. Given certain network load distribution, the OpenDSS model [19] is solved twice in the harmonics mode – once with and once without perturbation to the load, i.e., $P(l, h)$ and $P(l, h) + \Delta P(l, h)$. Then $\omega(br, l, h)$ and $\mu(br, l, h)$ are approximated by the ratios of the TDD and THD changes against the active power consumption change $\Delta P(l, h)$. The same power factor is assumed for the load both before and after the perturbation. This study finds that the harmonic sensitivity factors can be either positive or negative, depending on the presence of Triplen harmonics in the spectrum of load l.

B. Frequency and Voltage Dips during Motor Starting

Large motor starting can cause voltage dips across the microgrid due to high motor inrush currents. The problem is aggravated when the motor is in duty cycle operation. The generator's capability to quickly recover from the voltage dip (ideally within a few seconds) is an essential requirement for the microgrid power quality, especially when sensitive loads are present.

C. Regeneration Load

For certain motor loads such as the elevators, the power system network should be able to absorb the power produced during braking. In microgrid standalone operation, there must be other loads connected in the microgrid to absorb excess power as the DGs' ability to absorb power is limited.

D. Phase balancing

Single phase loads are very prevalent in the microgrid. Although there were efforts to evenly distribute them during the system design, load imbalance among the phases will still occur in operation. Load imbalance will result in high negative sequence current, resulting in overheating of the synchronous DG armature coils.

In recent research studies, primary control techniques have been proposed to improve the power quality issues in microgrids [14, 15]. Many of the proposed controls involve power electronics devices such as the active harmonic filters, and are applicable in Building Microgrids. In practice, the primary controls for managing power quality may or may not be available in the microgrid depending on the existing implementation and economic justifications for equipment upgrade as the power quality problems only become significant during the microgrid standalone operation. Nonetheless, when power quality requirements are given adequate considerations during the energy scheduling of tertiary control, they can be effectively managed. In other words, harmful device interactions should be identified and avoided during energy scheduling so that the device power quality requirements are met in the energy schedule.

V. THE BUILDING MICROGRID ENERGY SCHEDULING ALGORITHM

Distinct building energy management policies can lead to different energy scheduling strategies in the commercial buildings. For example:

i. The building operator and the building occupants can belong to a single economic entity with common economic interest.
ii. The building operator and the building occupants can belong to multiple economic entities, and have competing economic interests as energy suppliers and consumers.

With the single economic entity, the building energy scheduling is mainly concerned with prioritizing equipment and appliance operations while considering realistic supply costs and values of lost energy services. With multiple economic entities, however, the building energy scheduling would likely involve competitive auctions such as the First Price auction. In the First Price auction, sealed bids are submitted to offer or request energy services. The bids are then cleared at as-bid prices. The decision outcomes under either economic policy should maximize the total welfare of energy services, i.e., the end-user's energy valuation less the supplier's production cost according to the bids.

The energy scheduling algorithm proposed in this study should support the energy scheduling decisions under either building energy policy. In the MAS based framework, the Energy Manager agent performs central energy scheduling upon receiving bids from the energy supplier agents and energy consumption device agents. The algorithm determines the optimal operation schedule of the building energy supply resources and load equipment over the planning time horizon for maximum total welfare. At the same time, all physical operating requirements of the microgrid are considered, including the power quality requirements.

It is also noted that the Building Microgrid can operate under either the economic or emergency condition. In economic operation (e.g., when grid is available), the microgrid has abundant energy supply to meet demand; in emergency operation (e.g., during grid outage), energy supply is scarce and may not fully meet demand. Under both operating conditions, the microgrid can operate in either the grid-connected or standalone mode. And for the different operating conditions, the energy suppliers and consumers may use different bidding strategies. In this study, it is assumed that the associated agents submit two sets of bids, one for economic operation and the other for emergency operation. The energy scheduling algorithm for clearing the bids, however, should have similar formulation for either operating condition.

In the following discussion, three groups of supply and demand entities are considered: Grid, distributed generation resources and the building equipment and appliances. The bid parameters from each agent consist of two parts: One part describes the operational characteristics and requirements of the associated device; the other part represents the willing-to-sell/buy prices of energy. All bid parameters are hourly variant.

A. Grid Bids

i. *Operational parameters*: For the grid g in operating hour h, the maximum and minimum grid power import to the Building Microgrid are $P_{max}(g, h)$ and $P_{min}(g, h)$ in kW.

ii. *Economic parameters*: The grid energy price is $C(g, h)$, in \$/kW·hour or \$/kWh. For ease of notation and without the loss of generality, single block bid price curves are assumed throughout the following discussion.

B. DG Bids

i. *Operational parameters*: For DG r in hour h, the maximum and minimum power output are $P_{max}(r, h)$ and $P_{min}(r, h)$ in kW. The DG's maximum tolerance to current TDD is $I_{tdd\_Max}(r)$ in percentage, the power factor rating $Pf(r, h)$, and minimum run time $T_{min\_run}(r)$ in hours.

ii. *Economic parameters*: For DG r in hour h, the DG energy supply cost is denoted by $C(r, h)$, in \$/kWh. It represents the unit quantity price at which the DG is willing to produce. In addition, the generation startup cost is denoted $C_{st}(r)$ and no load cost $C_{nl}(r)$.

C. Load Bids

i. *Operational parameters*: For load l in hour h, the maximum and minimum power consumptions are represented by $P_{max}(l, h)$ and $P_{min}(l, h)$ in kW. When load l represents an individual equipment, $P_{max}(l, h) = P_{min}(l, h) =$ equipment kVA rating $\times$ load operating power factor $Pf(l)$. When l represents an equipment aggregate, the power consumption can potentially be dispatched so that $P_{max}(l, h) \geq P_{min}(l, h)$. Also, let $T_{min\_run}(l)$ be the minimum run time requirement of the load in hours. The other operational parameters are as

follows: the load harmonic spectrum $H(l)$ is represented by a set of harmonic frequencies and the corresponding RMS in per unit (in reference to the base frequency component): $\{(60, 100), (120, I_{120}), (180, I_{180}), \ldots\}$; the bid of a sensitive load also includes the operating ranges of voltage and frequency in per unit: $[V_{low}(l), V_{high}(l)]$; and the maximum tolerance for voltage THD of a sensitive load is $V_{max\_thd}(l)$. If a load is of the regeneration type, the minimum microgrid loading level required by the regeneration load is denoted as $L_{regen}(l)$.

ii. *Economic Parameters*: For load l in hour h, the willing to buy price is denoted by $C(l, h)$, in \$/kWh.

D. Decision Variables

In this study, it is assumed that all distributed generation resources and/or loads have minimum power output or consumption levels once energized to operate. This modeling need is due to the small capacity scale of the micogrid, and the fact that device on and off operations can create measurable discrete changes in the load curve. Binary decision variables are therefore required to represent the device on and off status. For DG r, load l, BESS unit es in an operation hour h, the binary decision variables are:

- $On(r, h)$: 1 for the resource on status and 0 otherwise.
- $On(l, h)$: 1 for the load on status and 0 otherwise.
- $ST(r, h)$: 1 if the resource has a startup and 0 otherwise.
- $SD(r, h)$: 1 if the resource has a shutdown and 0 otherwise.
- $Chr(es, h)$: 1 if the BESS unit is charging and 0 otherwise.
- $DisChr(es,h)$: 1 if the BESS unit is discharging and 0 otherwise.

Meanwhile, the continuous variables are the following.

- $P(r, h)$: Active power output of a resource, in kW.
- $P(l,h)$: Active power consumption of a load, in kW.
- $P(es, h)$: Charging rate of the BESS unit, in kW. Positive if charging; negative if discharging.
- $UpRsv(r, h)$ and $DnRsv(r, h)$: Up and down operating reserve procured on a distributed generation resource.
- $SOC(es, h)$: BESS state of charge at the beginning of the hour. $0 \leq SOC(es, h) \leq 1$.

E. Mixed Integer Programming (MIP) Algorithm

The objective cost function is to maximize the total demand values less the costs of supply, over the study time horizon:

$$\text{Maximize} \left\{ \begin{array}{c} \sum_{l,h} P(l,h) \cdot C(l,h) - \\ \left(\sum_{h} P(g,h) \cdot C(g,h) + \sum_{r,h} P(r,h) \cdot C(r,h) \right) - \\ \left(\sum_{r,h} C_{st}(r,h) \cdot ST(r,h) + \sum_{r,h} C_{nl}(r,h) \cdot On(r,h) \right) \end{array} \right\} \quad (5)$$

The operating constraints are described as follows.

a. Microgrid active power balance constraint:

$$P(g,h) + \sum_{r} P(r,h) = \sum_{l} P(l,h) + P_{loss}(h) \quad (6)$$

where parameter P_{loss} is the hourly total active power loss.

b. Reactive power balance constraint:

$$Q(g,h) + \sum_{r} Q(r,h) = \sum_{l} Q(l,h) + Q_{loss}(h) \quad (7)$$

where parameter Q_{loss} is the hourly total reactive power loss.

c. Operating reserve constraint – the total operating reserve procurement should meet the specified system requirement:

$$\sum_{r} UpRsv(r,h) \geq UpRsvRq(h) \quad (8)$$

$$\sum_{r} DnRsv(r,h) \geq DnRsvRq(h) \quad (9)$$

The operating reserves are necessary for both frequency regulation in the Building Microgrid, and coping with unexpected loss of generation or load changes. The bi-directional operating reserves procured on generation resources are $UpRsv(r, h)$ and $DnRsv(r, h)$. And the bidirectional system operating reserve requirements are $UpRsvRq(h)$ and $DnRsvRq(h)$.

d. Phase balance constraints to ensure that the active power scheduled among the three phases should be within close proximity:

$$\left| \sum_{l} P(l,h) \cdot PhA(l) - \sum_{l} P(l,h) \cdot PhB(l) \right| \leq P_{unb\_max} \quad (10)$$

$$\left| \sum_{l} P(l,h) \cdot PhA(l) - \sum_{l} P(l,h) \cdot PhC(l) \right| \leq P_{unb\_max} \quad (11)$$

$$\left| \sum_{l} P(l,h) \cdot PhB(l) - \sum_{l} P(l,h) \cdot PhC(l) \right| \leq P_{unb\_max} \quad (12)$$

where maximum power imbalance P_{unb_max} is a pre-defined system parameter, dependent on the DG's unbalanced load capability, and the grid code requirement. Parameters PhA, PhB, PhC represent the allocation factors of load l to phases A, B and C in percentages.

e. Resource reserve procurement constraint:

$$P(r,h) + UpRsv(r,h) \leq On(r,h) \cdot P_{max}(r,h) \quad (13)$$

$$P(r,h) - DnRsv(r,h) \geq On(r,h) \cdot P_{min}(r,h) \quad (14)$$

f. Generation resource reactive power limit constraint to ensure that the power factor of a DG resource should not exceed its rating:

$$On(r,h) \cdot P_{min}(r,h) \cdot \frac{\sqrt{1 - Pf^2(r,h)}}{Pf(r,h)} \leq Q(r,h) \leq$$

$$On(r,h) \cdot P_{max}(r,h) \cdot \frac{\sqrt{1 - Pf^2(r,h)}}{Pf(r,h)} \quad (15)$$

g. BESS unit charging and discharging constraints:

$$Chr(es,h) + DisChr(es,h) \leq 1 \quad (16)$$

$$P(es,h) \leq Chr(es,h) \cdot P_{max\_ch}(es) - DisChr(es,h) \cdot P_{min\_disch}(es) \quad (17)$$

$$P(es,h) \geq Chr(es,h) \cdot P_{min\_ch}(es) - DisChr(es,h) \cdot P_{max\_disch}(es) \quad (18)$$

$$0 \leq SOC(es,h) \leq 1 \quad (19)$$

$$SOC(es,h) = SOC(es,h-1) + \frac{P(es,h-1) \cdot HourLength}{E_{max}(ess)} \quad (20)$$

where parameters P_{max_ch}, P_{min_ch}, P_{max_disch}, P_{min_disch} in kW are the maximum and minimum charging and discharging rates of the BESS; E_{max} is the maximum energy storage capacity in kWh.

h. Load active power consumption constraints:

$$On(l,h) \cdot P_{\min}(l,h) \leq P(l,h) \leq On(l,h) \cdot P_{\max}(l,h) \quad (21)$$

i. Load reactive power consumption constraints:

$$Q(l,h) = P(l,h) \cdot \frac{\sqrt{1 - Pf^2(l)}}{Pf(l)} \quad (22)$$

j. Sensitive device current harmonics constraints:

$$I_{previous\_tdd}(br,h) + \sum_l \omega(br,l,h) \cdot \left(P(l,h) - P_{previous}(l,h)\right)$$
$$\leq \mu \cdot I_{\max\_tdd}(br,h) \quad (23)$$

where br is the terminal branch of the sensitive device; $\omega(br, l, h)$ is the TDD sensitivity factor defined in section IV; and $I_{max\_tdd}(br, h)$ is the maximum TDD level allowed for the sensitive device operation. Parameters $I_{previous\_tdd}$ and $P_{previous}$ represent the current TDD and power dispatch from a previous iteration of solution. Parameters $V_{previous\_thd}$ and $P_{previous}$ in equation (25) are similarly defined. Constraints (23) through (26) are only enforced after initial optimal solution(s) have been obtained. Parameters $\mu \cong 1$ and $\eta \cong 1$ (in constraint 25) are heuristic parameters that help to facilitate the solution. This iterative solution strategy is further explained in section VI. In this study, the device sensitive to current harmonics are primarily the DGs. Therefore, the right hand side of constraint (23) can be replaced through:

$$I_{\max\_tdd}(br,h) = I_{\max\_tdd}(r) \cdot On(r,h) + M \cdot \left(1 - On(r,h)\right) \quad (24)$$

for all r, and a sufficiently large number M.

k. Sensitive device voltage harmonics constraints:

$$V_{previous\_thd}(n,h) + \sum_l \mu(n,l,h) \cdot \left(P(l,h) - P_{previous}(l,h)\right) \leq$$
$$\eta \cdot V_{\max\_thd}(n,h) \quad (25)$$

where n is the terminal node of the sensitive device; $\mu(n, l, h)$ is the THD sensitivity factor defined in section IV; and $V_{max\_thd}(n,h)$ is the maximum THD level allowed for the sensitive device operation. In this study, the devices sensitive to voltage harmonics are primarily the sensitive loads. Therefore, the right hand side of equation (25) can be replaced through:

$$V_{\max\_thd}(n,h) = V_{\max\_thd}(l) \cdot On(l,h) + M \cdot \left(1 - On(l,h)\right) \quad (26)$$

for each sensitive load l, its connected node n and a sufficiently large number M.

l. Regeneration load shutdown requirement constraint:

$$\sum_l P(l,h) \geq SD(l_r,h) \cdot L_{\min\_load}(l_r) \quad (27)$$

where l_r is a regeneration load. If l_r is also a duty cycle load, then decision variable $SD(l_r, h)$ should be replaced by decision variable $On(l_r, h)$ in (27).

m. Sensitive load voltage requirement constraint – This constraint is to ensure that excessive voltage drop as a result of motor starting does not occur during sensitive load operation. Let l_m be a motor load whose startup can cause the microgrid voltage to drop below the tolerance level of sensitive load l_s. Then:

$$On(l_s,h) + ST(l_m,h) \leq 1 \quad (28)$$

If l_m is also a duty cycle load, then variable $ST(l_m, h)$ should be replaced by variable $On(l_m, h)$.

n. Generation resource minimum run time constraint:

$$ST(r,h) - SD(r,h) = On(r,h) - On(r,h-1) \quad (29)$$
$$ST(r,h) + SD(r,h) = 1 \quad (30)$$
$$ST(r,h) \geq \frac{\left(\sum_{h1=h}^{h+T_{\min run}(r)-1} On(r,h1)\right)}{T_{\min\_run}(r)} \quad (31)$$

o. Load equipment minimum run time constraints are similarly formulated as (29), (30), and (31), with the element index changed from r to l.

VI. CASE STUDIES

The case studies are performed to demonstrate the effectiveness of the proposed energy scheduling algorithm in both managing power quality and achieving the economic objectives in the Building Microgrid operation. Three software tools are used in the simulation studies:

- AIMMS for the implementation of the optimization algorithm and solution [18].
- OpenDSS for network steady state harmonic analysis [19].
- PSCAD for the electromagnetic analysis [20].

The microgrid energy scheduling algorithm ((5)~(31)) is implemented in AIMMS with the CPLEX 12.5 solver. As illustrated by the flow chart in Figure 4, an optimal energy schedule solution is initially obtained without the constraints (23) through (26), (28) enforced. Then the initial energy schedules on both the loads and generation resources are evaluated for current TDD and voltage THD using the OpenDSS harmonic solver. If any TDD or THD violations against requirements occur, then the energy schedule solution is solved again with constraints (23) through (26) enforced and the TDD and THD sensitivity factors computed by the OpenDSS. The iteration continues until all harmonic distortions are controlled under requirement levels.
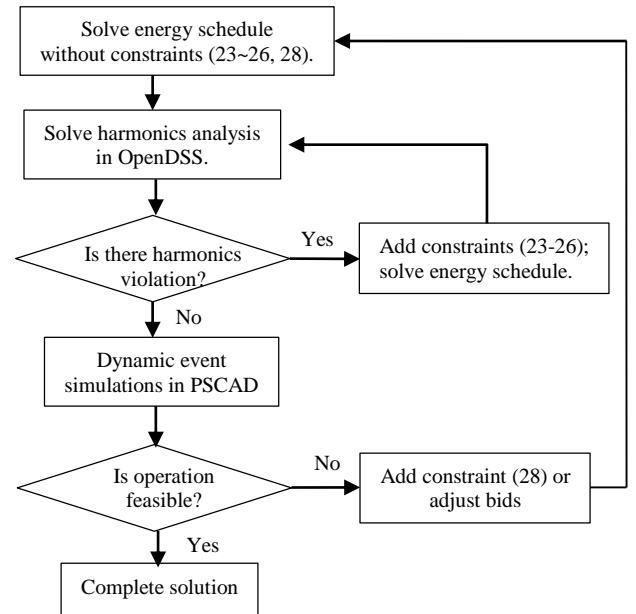
Figure 4: Energy Scheduling Algorithm Flow Chart

Also as illustrated in Figure 4, the PSCAD simulations are run after the energy schedule with harmonics mitigation has been obtained. The simulations are run to further validate the energy schedule against dynamic events. If any voltage or frequency violations, or system instability are found, new constraints such as constraint (28) can be created to reduce the impact of voltage or frequency deviation. Or, the bids are adjusted or removed to mitigate instability. The bid modifications can be made based on heuristic rules, or the building operator's manual input. During the PSCAD simulations, all primary controls are modeled with the abilities to follow secondary control setpoints as input.

A. System Physical Parameters

The percentages of linear loads, nonlinear loads and duty cycle motor loads are set be 10%, 60% and 30%, to represent a typical mix of loads in commercial buildings. The system operating reserve requirements $UpOprRq(h)$ and $DnOprRq(h)$ are set to be 40 kW, to cope with the potential volatile operation of the largest load; the system unbalanced loading tolerance P_{unb_max} is set to 60 kW, which is equal to 15% of combined active capacity of DG1 and DG2. The wind and solar generation data should reflect forecasts. In this study, the hourly wind and solar generation data at CWRU on a selected summer day (06/01/2014) are used to represent the forecasts. For the BESS unit, $P_{max\_chr} = P_{max\_dischr} = 40$ kW; $P_{min\_chr} = P_{min\_dischr} = 5$ kW; and $E_{max} = 80$ kWh. The power quality considerations include the following:

- Voltage and frequency deviations during motor starting and microgrid operational model transitions. According to the repeated PSCAD simulations on starting the 40 kW motor during the microgrid standalone operation, the voltage and frequency dips are less than 0.5% p.u. and 0.5HZ (Figure 5), which would not violate any of the sensitive load voltage requirements. Therefore, constraint (28) initially was not enforced.
- Motor breaking load requirement L_{min_load} is set to 40 kW.
- The current TDD of generator DG1 and DG2 are required to be less than 15% during the microgrid standalone operation.
- The voltage THD levels at sensitive loads are required to be less than 10%. The study considers one sensitive load, which is located 200ft downstream from transformer T_5.

Also in this study, predetermined hourly values are used for $P_{loss}(h)$ and $Q_{loss}(h)$ that represent the upper bounds of losses in the system. These values are calculated by the OpenDSS studies and represent a very small percentage of the total hourly loads.

B. Bid Parameters

When the DGs and loads belong to the same economic entity, the DG bids would reflect the realistic generation costs, and load bids reflect the realistic values of lost services. When the DGs and loads belong to multiple economic entities, competition would arise and the bids do not necessarily reflect the load's realistic valuation of the electricity service. In this study, a single economic entity is assumed and bid parameters are specified to reflect realistic operating capabilities, costs, and values of lost service. Also due to these assumptions, similar bid parameters are used for both the economic and emergency operations. These simplified test conditions allow the study to focus on the physical system modeling without elaborate discussions on bidding strategies.

The following table summarizes the grid energy prices and distributed generation resource bid parameters. Presumably, the grid energy prices should be results of the electricity market price forecast.

Table 1: Microgrid Generation Supply Bids

	$P_{max}(\cdot,h)$	$P_{min}(\cdot,h)$	$C(\cdot,h)$	$C_{st}(\cdot,h)$	$C_{nl}(\cdot,h)$
Grid	1600 kW	0	<\$3/kWh	0	0
DG1	200 kW	50 kW	\$0.90/kWh	\$300	\$100/h
DG2	200 kW	50 kW	\$0.91/kWh	\$300	\$100/h
Solar	40 kW	0 kW	\$0.01/kWh	0	0
Wind	60 kW	0 kW	\$0.01/kWh	0	0

The following general rules have been used in selecting the load bid parameters. Among the 75 loads modeled with capacities ranging from a few kWs to a maximum of 40 kW, the bidding prices of the loads are to reflect the values of lost service, between \$0.01 and \$500 per kWh.

The studies of two essential energy scheduling cases are presented in the following, one for buildings-to-grid economic operation and the other for standalone emergency operation. The initial energy scheduling solutions with harmonic mitigations are presented in section *C*. Three most impactful dynamic events in both energy schedules are identified and studied in section *D*.

C. Energy Scheduling Case Studies

C1. Case Study I: Buildings-to-Grid Economic Operation

This case study examines the 24-hour microgrid energy schedules corresponding to 3 grid energy price profiles, in which the prices mainly differ in three peak hours, hours 14, 15 and 16.

After the initial energy schedules are obtained from the AIMMS algorithm solution, they are evaluated by OpenDSS for harmonic distortions. The energy schedules for two of the three grid price profiles required grid-tied operation of the microgrid through all hours, when no violations of current TDD and voltage THD requirements are found. The energy schedule for the third price profile required microgrid standalone operation during the three peak hours, and both current TDD and voltage THD requirements are found violated during the standalone operation. Constraint (23) through (26) are activated and 2 iterations between the AIMMS algorithm and OpenDSS harmonic solver were required to mitigate the current TDD and voltage THD violations. In the final energy schedule, the current TDD of the DG is below 14.3% which meets the 15% requirement. The final energy schedule solution also uncommitted the sensitive load during the standalone operation hours, as the lost opportunity cost for mitigating voltage THD for the sensitive load is much higher than the sensitive load bidding price of \$1/kWh.

For the three pricing profiles, the cleared hourly grid imports are plotted against the grid hourly energy prices as in the top charts in Figure 5. It can be seen that as the grid energy price rises in the peak hours (hours 14, 15 and 16), the microgrid starts deploying onsite DGs to reduce energy cost. For pricing profile *c* (Figure 5 (*c*)-(*c'*)), the energy scheduling solution results in the microgrid standalone operation in hours 14, 15 and 16.

C2. Case Study II: Standalone Emergency Operation

In this scenario, grid outage is assumed and the microgrid is in emergency standalone operation where the DGs cannot meet all the load demand in the microgrid.
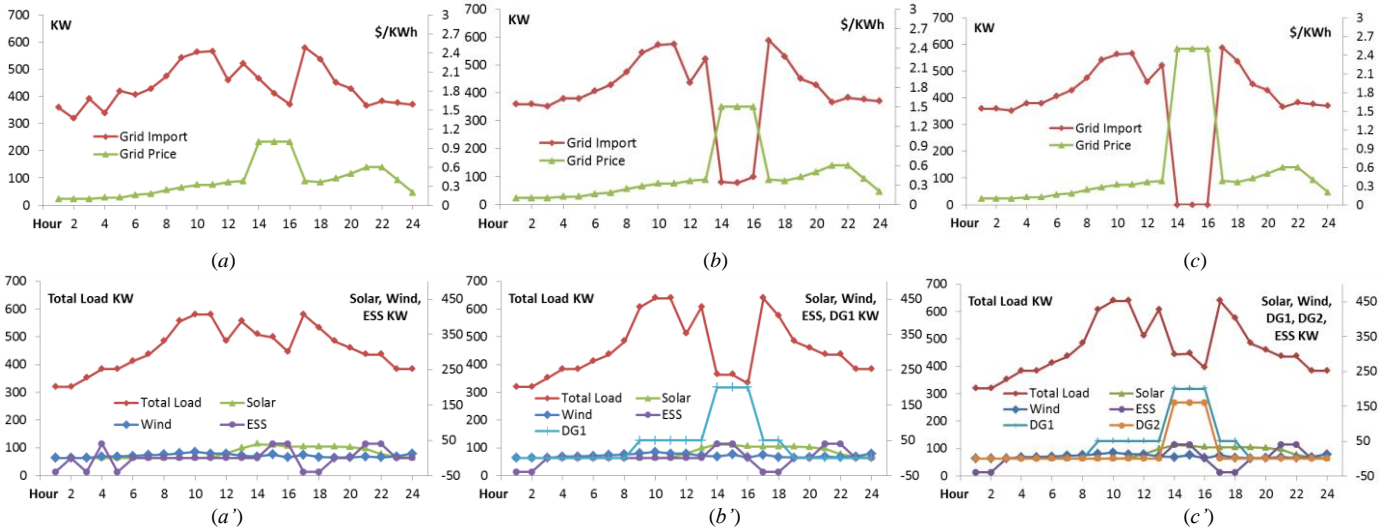
Figure 5: Microgrid energy scheduling under three grid hourly price profiles: (*a-a'*), (*b-b'*), (*c-c'*).
(Top charts are grid imports plotted against 3 grid pricing profiles.
Bottom charts show the corresponding dispatch of DG against total load cleared on the microgrid.)
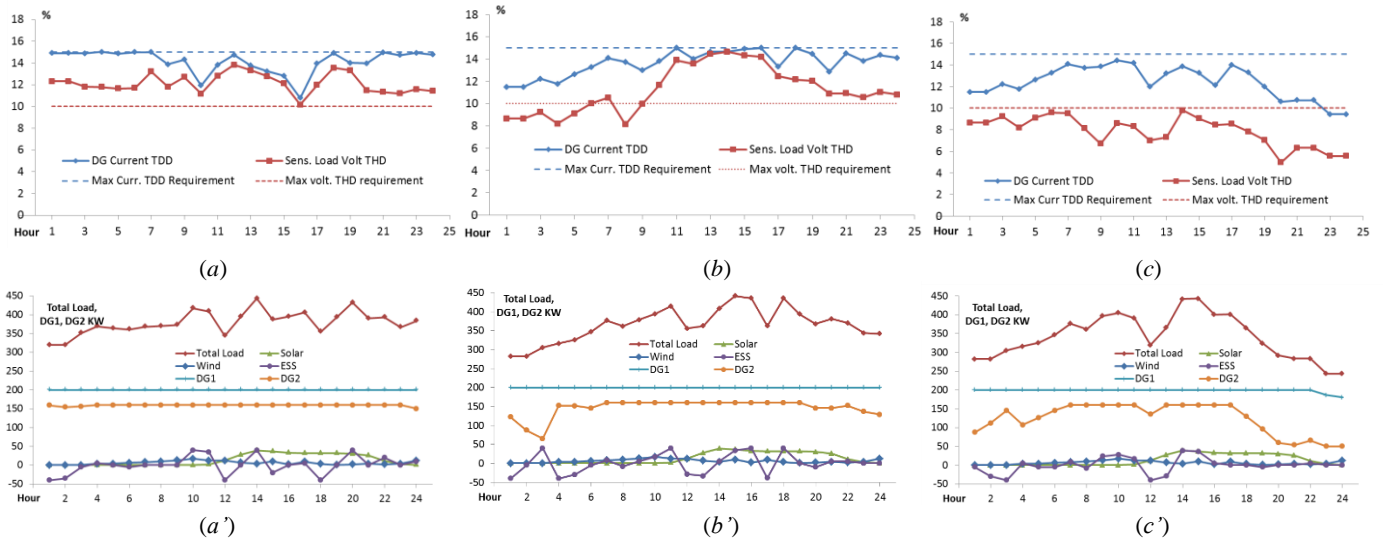
Figure 6: Mitigation against current TDD and voltage THD during microgrid standalone operation
(Top charts show current TDD and voltage THD under the three prices offered by the sensitive load: (a) $1, (b) $220, (c) $500 per kWh.
Bottom charts show the corresponding dispatch of DG against total load cleared on the microgrid.)

During the energy schedule solution, the grid bid commitment variable $On(g, h)$ is forced to be zero throughout the hours to enable microgrid standalone operation. Three scenarios are created with different 24-hour bidding prices of the sensitive load. The sensitive load also has a minimum run time of 8 hours.

In the initial energy schedule solutions, the current TDD and voltage THD violations are seen in most hours due to the loss of power grid as a stiff source. The final energy schedule solutions are obtained within 2 iterations between the AIMMS model and OpenDSS harmonic solver. As the study results of Figure 6 show:

a. When the sensitive load bids in $1/kWh for the 24 hours, it isn't committed as the lost-opportunity cost for mitigating voltage harmonics on its behalf is much higher than its willing-to-pay bid price.

b. When the sensitive load bids in $220/kWh for the 24 hours, it is committed for hours 1 through 8. The energy scheduling algorithm only mitigated the voltage THD on its behalf during these hours.

c. When the sensitive load bids in $500/kWh for the 24 hours, it is committed throughout the 24 hours except hour 16 and the energy scheduling algorithm successfully mitigated the voltage THD during all hours of commitment.

It is also seen that the energy scheduling algorithm is able to successfully mitigate the current TDD for both DG1 and DG2 during all hours of microgrid standalone operation. For the three pricing scenarios, the total cleared loads have undergone modest changes. The energy scheduling algorithm mainly swapped loads of high harmonic contents with loads of low harmonic contents.

It is important to note that in both case studies, the mitigation of harmonic distortion impact has been carried out by
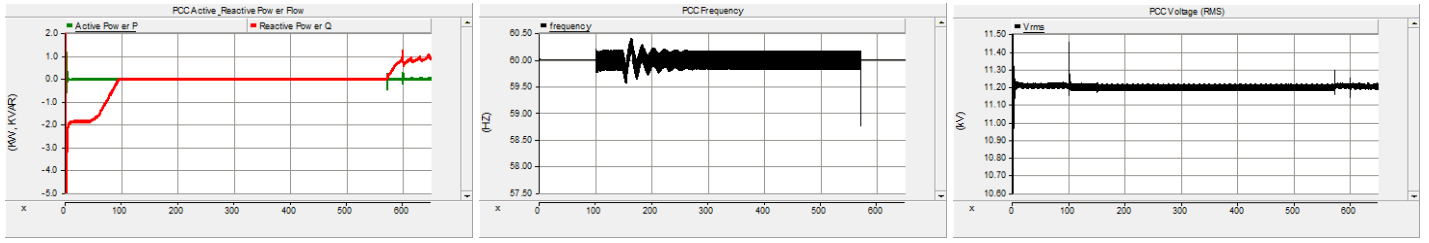
Figure 7: PCC voltage and frequency responses during microgrid operation mode transitions
(Grid-tied to standalone transition occurs at 100s and standalone to grid-tied transition at 570s.)
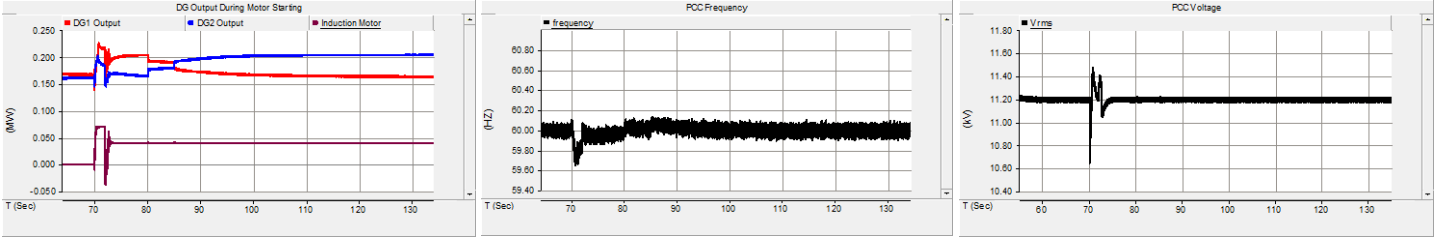
Figure 8: DG generation output, system voltage and frequency responses during induction motor starting in standalone microgrid
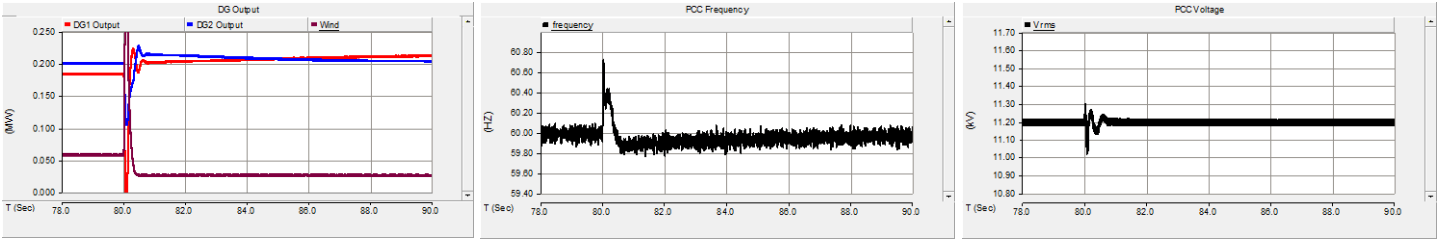
Figure 9: DG and wind generation output, system voltage frequency and responses during wind transient in standalone microgrid

reducing the loads of high harmonics contents. In other words, only positive sensitivity factors of equations (3) and (4) have been applied in constraints (23) through (26). Mitigation through negative sensitivity factors (i.e., through harmonic cancellation) has led to uncertain outcomes. A further analysis of the sensitivity factors as defined by (3) and (4) will be required to fully address the observations.

For the scenarios solved in both case studies I and II, the MIP solution times of the energy scheduling algorithm are under 5 seconds with zero MIP gap. The total number of variables are about 7.7×10^3, of which 5.5×10^3 are integer variables. The total number of constraints are 9.6×10^3.

D. Dynamic Event Simulations

A review of the energy schedules in case studies I and II above identifies planned operation mode transitions, motor starting and wind transients as among the most impactful dynamic events in the microgrid standalone operation. The following simulated system responses during these events involve coordination between primary and secondary controls for ensuring frequency and voltage stabilities. The simulations are performed with a PSCAD model built based on the system of Figure 1.

D1. Planned Transitions between Operation Modes

In the simulation for the planned transition of microgrid operation from the grid-connected to the standalone mode, the interconnection switch at the PCC is opened when the active and reactive power transfers at the PCC are managed to the near-zero

levels by the secondary control dispatch of P/Q setpoints for DG1 and DG2. During the transition from the standalone mode to grid-connected mode, on the other hand, the secondary control provides frequency and voltage setpoints for DG1 and DG2 so that the differences in voltage magnitude and phase angle between the microgrid and grid at the PCC are nearly zero. Figure 7 shows the simulation results on the active and reactive power flow control, and the smooth voltage and frequency responses at the PCC during the operation transition events.

D2. Induction Motor Starting

In this simulation study of the microgrid standalone operation, DG1 is scheduled to provide operating reserve and placed on the voltage/frequency regulation mode. DG2 is in the P/Q control mode to follow setpoints. In the simulation, the 40 kW induction motor is started at time t = 70s. The secondary control algorithm instructs DG2 to increase output by 40 kW according to energy schedule. This is carried out by ramping of the gas turbine twice, once at t = 80s and once at t = 85s. As shown in Figure 8, both DG1 and DG2 respond to the load increase initially due to P-f droop control (80 – 90s). Then DG2 continues to ramp up to pick up the 40 kW motor load while DG1 returns to the output position as of prior to the event. The system frequency and voltage are maintained at nominal levels following the event.

D3. Wind Transient

During this simulation study, wind speed suddenly drops from 12 m/s to 9 m/s resulting in a 25-kW loss of wind generation. This is considered a contingency event and the

operating reserve carried by DG1 is expected to make up the lost generation. As shown in Figure 9, both DG1 and DG2 initially responded due to *P-f* droop control. Then DG1 that is placed on frequency and voltage regulation gradually picks up the lost generation and DG2 returns to the same output position as before the event. The system frequency and voltage are maintained at nominal levels after the incident.

Some of the primary control schemes of the above simulation studies are shown earlier in Figure 2. The secondary control setpoint changes in time are hardcoded in PSCAD. To show the primary and secondary control responses in the same multiple-second time window, the inertia of gas turbines has been modified for faster responses. In actual implementation, the secondary control setpoints would be algorithmically determined based on the energy schedule and real-time measurements and communicated by agents. Also, device response time to setpoint instructions can take many minutes.

E. Discussions

The case studies have demonstrated the effective mitigation of power quality issues in the Building Microgrid operation through coordination among the hierarchical controls. In particular, the issues are identified and managed in the energy scheduling algorithm where both the steady state and dynamic simulations of the microgrid operation are integral steps for validating and correcting the energy schedules against power quality requirements. The energy scheduling algorithm can serve to manage energy procurement in either competitive or non-competitive settings of building operation. While the grid energy prices are obtained from the electricity market price forecast [6], other supplies and demands are represented by bids that are cleared by the energy scheduling algorithm. The case studies also show that in commercial building operation, energy transactions from equipment and appliances can be first aggregated through a central algorithm that achieves local operational and economic objectives. The Building Microgrid can work as an ideal physical infrastructure to facilitate the process. The aggregate bids, as indicated by the top charts in Figure 5, can be communicated to the upper tier level energy management in the transaction-based framework, such as a distribution system operator.

VII. CONCLUSIONS

Power quality issues are outstanding in the standalone operation of small capacity microgrids such as those serving small to medium size commercial buildings. This study has proposed a MIP-based energy scheduling algorithm where the power quality requirements on voltage and frequency deviations, and harmonic distortions are enforced as constraints. While attempting to realize maximum total welfare, the algorithm coordinates the operation schedules of nonlinear and motor loads so that power quality requirements of sensitive equipment and appliances are met during operation. Iterative solutions with the steady state and dynamic analysis tools such as the OpenDSS and PSCAD are required in order to obtain such energy schedules. The proposed algorithm can be implemented in a commercial building environment where a BAS is present, and with distributed generation and loads managed by device agents on an MAS platform. In the transaction-based framework, Building Microgrids can effectively fulfill the functional role of

building end-use site to facilitate building to grid integration. Meanwhile, this proposed algorithm can serve to aggregate the energy transaction bids of the building devices before communicating to the upper tier level energy management.

VIII. REFERENCES

[1] IEEE Standard 1547.4 - IEEE Guide for Design, Operation, and Integration of Distributed Resource Island Systems with Electric Power Systems, IEEE, 2011.

[2] C. Marnay, G. Venkataramanan, M. Stadler, A.S. Siddiqui, R. Firestone, Bala Chandran, "Optimal Technology Selection and Operation of Commercial-Building Microgrids," IEEE Trans. on Power Systems, Vol. 23 (3), Aug. 2008, pp. 975-982.

[3] X. Guan, Z. Xu and Q-S Jia, "Energy-Efficient Buildings Facilitated by Microgrid," IEEE Trans. on Smart Grid, Vol. 1 (3) Dec. 2010, pp. 243-252.

[4] L.G. Meegahapola, D. Robinson, A.P. Agalgonkar, S. Perera, P. Ciufo, "Microgrids of Commercial Buildings: Strategies to Manage Model Transfer from Grid Connected to Islanded Mode," IEEE Trans. on Sustainable Energy, pre-publication available online.

[5] Buildings to Grid Integration, Office of Energy Efficiency & Renewable Energy, Department of Energy, http://energy.gov/eere/buildings/buildings-grid-integration.

[6] P. Huang, J. Kalagnanam, R. Natarajan, M. Sharma, R. Ambrosio, D. Hammerstrom, R. Melton, "Analytics and Transactive Control Design for the Pacific Northwest Smart Grid Demonstration Project," 2010 First IEEE Smart Grid Communications, Oct 2010, Gaithersburg, MD.

[7] Reference Guide for a Transaction-Based Building Controls Framework, Pacific Northwest National Laboratory, April 2014.

[8] J. Iverson, "How to Size a Genset: Proper Generator Set Sizing Requires Analysis of Parameters and Loads," Cummins Power Generation, 2007.

[9] M. Hong, X. Yu, W.J. Culver, K.A. Loparo, "Optimal Control of Distributed Generation in a Campus Grid," IEEE EnergyTech 2014.

[10] A. Priyadharshini, N. Devarajan, A.U.Saranya, R. Anitt, "Survey of Harmonics in Non-linear Loads," Int. J. Recent Technology and Engineering, ISSN 2277-3878, Vol. 1 (1), Apr. 2012.

[11] Electrical Load Impact on Generator Sizing, Cummins Power Generation, 2004.

[12] A. Bidram and A. Davoudi, "Hierarchical Structure of Micogrids Control System," IEEE Trans. on Smart Grid, Vol. 3 (4), Dec 2012, pp. 1963 – 1976.

[13] S. Latipamula, "PNNL VOLTTRON™ Application Development," DOE Building Technologies Office: Technical Meeting on Software Framework for Transactive Energy, July 23-24, 2014.

[14] IEEE Standard 519-1992 – IEEE Recommended Practices and Requirements for Harmonic Control in Electrical Power Systems, IEEE, 1992.

[15] M. Prodanović and T.C. Green, "High-quality power generation through distributed control of a power park microgrid," IEEE Trans. on Ind. Electron., vol. 53, Oct. 2006, pp. 1471 – 1482.

[16] Y.W. Li, D.M. Vilathgamuwa, and P.C. Loh, "A Grid-Interfacing Power Quality Compensator for Three-Phase Three-Wire Microgrid Applications," IEEE Trans. on Power Electron., Vol. 21, Jul. 2006, pp. 1021 – 1031.

[17] R.C. Dugan, M.F. Mcgranaghan, S. Santoso, H.W. Beaty, Electrical Power Systems Quality (3rd Edition), Mcgraw-Hill, 2012.

[18] AIMMS, http://business.aimms.com/.

[19] OpenDSS, Smart Grid Rsource Center, EPRI, http://smartgrid.epri.com/SimulationTool.aspx.

[20] Power System Computer Aided Design (PSCAD), Manitoba HVDC Research Center, https://hvdc.ca/pscad/.